Original scientific paper

CARBON NANOTUBE UNDER PULSED PRESSURE

Marat A. Ilgamov[1,2,3], Aigul A. Aitbaeva[3], Igor S. Pavlov[4,5], Sergey V. Dmitriev[6,7]

[1]Blagonravov Institute of Mechanical Engineering,
Russian Academy of Sciences, Moscow, Russia
[2]Institute of Mechanics and Engineering, KSC, Russian Academy of Sciences, Kazan, Russia
[3]Institute of Mechanics, UFRC, Russian Academy of Sciences, Ufa, Russia
[4]Institute of Applied Physics, Russian Academy of Sciences, Nizhny Novgorod, Russia
[5]Lobachevsky State University of Nizhny Novgorod, Nizhny Novgorod, Russia
[6]Institute of Molecule and Crystal Physics, UFRC, Russian Academy of Sciences, Ufa, Russia
[7]Department of Equipment and Technologies of Welding and Control,
Ufa State Petroleum Technological University, Ufa, Russia

Abstract. *The radial dynamics of a single-walled zigzag carbon nanotube under pulsed pressure is studied. Uniform external pressure is applied instantly, then remains constant for a certain time, and then is instantly released. This loading scheme allows one to consider a carbon nanotube under plane strain conditions and replace it with a circular ring formed by one zigzag row of carbon atoms. The bending deformation of the ring in its plane is described by an equation based on the Kirchhoffs hypothesis. An effective parameter is used, including the bending stiffness of the ring and areal density. The regimes of oscillatory motion and exponential growth of radial displacements are investigated depending on the magnitude and duration of the applied pressure. Alternatively, the ring is analyzed in terms of a molecular dynamics model with a reduced number of degrees of freedom, taking into account the plane strain conditions. With the help of molecular dynamics, the limits of the thin shell theory are established. For (n, 0) CNTs with n > 15, in the regime of small-amplitude vibrations, the discrepancy between the continuum model and molecular dynamics calculations does not exceed 5% and decreases with increasing n.*

Key words: *Carbon nanotube, Molecular dynamics, Shell theory, Pulsed pressure, Natural frequencies*

1. INTRODUCTION

Free and forced vibrations of carbon nanotubes (CNTs) have been analyzed in a number of studies [1-13] because they affect the operation of nano-devices such as sensors, actuators, etc.

The physical and mechanical characteristics of CNTs, including their behavior under static and dynamic loading, are often investigated using the methods of molecular dynamics and continuum mechanics [1-5]. In the latter case, the effective dimensions of CNTs, effective elastic and mass parameters are introduced. In this work, the molecular dynamics and the theory of thin shells with a parameter determined from the comparison of natural frequencies within the framework of these models are used.

The effect of a uniform dynamical pressure on a single-walled CNT is considered. The effect of pressures on CNTs is discussed in reviews [6, 7]. There are experimental studies of the dynamic, structural and electrical properties of single-walled and multi-walled CNTs, depending on the uniform static and dynamic pressure [8-13]. These works also consider theoretical modeling within the framework of molecular dynamics and continuum mechanics. The deformation of isolated CNTs under static pressure is analyzed, which is a necessary step in studying the complex behavior of a CNT bundle under dynamic pressure. It has been shown [10, 11] that with an increase in static pressure up to $p_1 \approx 3D/R$, the CNT cross-section acquires the shape of an ellipse (here D is the CNT wall bending stiffness and R is the CNT radius). In the elliptic state, the radial stiffness of the CNT decreases by two orders of magnitude [11]. Further increasing the pressure up to $p_2 \approx p_1[1-\ln(F_2/F_1)]$ results in a cross-sectional shape with two opposite points of zero curvature. With a further increase in pressure up to $p_3 \approx p_1[1-\ln(F_3/F_1)]$, the deformation of the cross-section increases and the electrical properties of the CNT change (transition to semiconductor state takes place). Here F_1, F_2 and F_3 are the cross-sectional areas corresponding to the pressures p_1, p_2 and p_3. For a single-walled armchair CNT (10, 10), $p_1=1.55$, $p_2=1.75$ and $p_3=2.2$ GPa [10].

The static stability and deformations of thin elastic circular rings under nonuniform pressures $p=p_0(1+q\cos\theta)$ were studied and it was found that the ring deforms only in a doubly symmetric fashion, while static buckling into an asymmetric pattern was not observed [14].

Vibrational properties of long hollow cylindrical shells interacting with the external medium were analyzed in the works [15, 16].

The structural transformations in CNT bundles during laser compression and the resulting oscillations have been considered [8, 9, 12]. In these and other works [17, 18], Raman spectroscopy is widely used in experimental studies. The behavior of CNTs was studied experimentally at different distances between them in the bundle (from 1.5 to 1.7 nm). In [13], the change in the properties of a single multilayer CNT under shock compression through the surrounding elastic material was studied.

The radial breathing mode frequency of various zigzag and armchair CNTs with radii between 3.5 and 8.1 Å have been determined using the first-principles calculations [19]. Dispersion relations for long-wavelength phonons in graphite and achiral single-walled CNTs have been analyzed using a continuum model [20]. Analysis of vibration behavior of carbon nanomaterials is important for design of nano-mass, nano-force and strain sensors [21-29] as well as microelectromechanical systems for various purposes [7, 30].

Dynamic loading of carbon nanomaterials is considered in solving important problems related to the damping of shocks and vibrations as well as projectile protection. Molecular dynamics simulations and experiments were conducted to study energy dissipation in CNT films under ballistic impact [31, 32, 33]. Energy dissipation by collapsing CNTs in the bundle under shock loading was analyzed in the work [34].

In this work, we analyze the response of single-walled CNTs to a uniform dynamic pressure within the framework of the theory of thin shells and molecular dynamics.

2. PROBLEM STATEMENT

It is assumed that a time-varying external uniform excess pressure $p(t)$ is applied at time $t=0$ to a single-walled zigzag CNT, which at $t<0$ is under the same external and internal pressure p_0 (for example, atmospheric pressure).

For a uniform pressure, zigzag CNT can be considered as a ring formed by single zigzag chain of carbon atoms (see Fig. 1). As the length of the valence bond, we take l=1.273Å which is slightly less than the experimental value in graphene, 1.4 Å, due to the effect of curvature of the CNT wall, especially for CNTs with a small radius. In the ring, the distance between the carbon atoms, projected onto the xy plane, is equal to $a=l\cos30°$=1.102 Å.
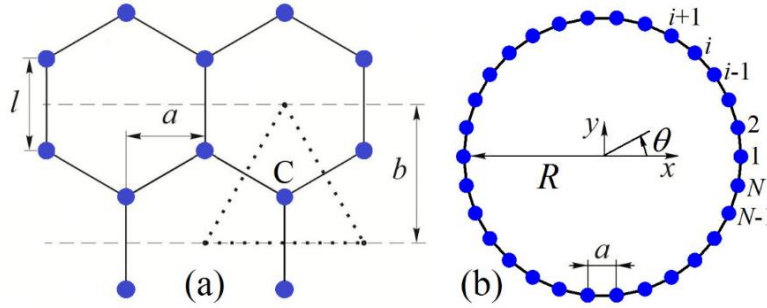
Fig. 1 (a) The structure of a zigzag CNT wall and (b) representation of the zigzag CNT by the chain model. The valence bond length is l=1.273Å, the distance $a=l\cos30°$=1.102 Å, CNT radius is R. Cross section of the zigzag CNT $(n,0)$ is presented by $N=2n$ carbon atoms numbered with the index i=1,…,N; the case of N=30 is shown in (b). A ring of width $b=3l/2$=1.91 Å is considered with periodic boundary conditions along the z axis. The area per one C atom S=2.105 Å^2 is shown by dotted lines (equilateral triangle).

A continuum mechanics model considers a ring formed by two cross sections at a distance $b=3l/2$=1.91 Å symmetrically relative to a zigzag row of carbon atoms. The radius R is determined from the equality

$$a = 2R\sin\frac{\pi}{N} , \qquad (1)$$

where N is the number of atoms forming the ring. Note that $N=2n$ for the zigzag CNT $(n,0)$ The area per atom is equal to S=2.105 Å^2. The mass of a carbon atom is M=1.99×10^{-26} kg

or M=12 a.m.u. Here we use angstroms, picoseconds, and electronvolt as units of measure for distance, time, and energy, respectively. In these units the carbon atom mass is M=1.244×10^{-3} eV·ps^2/Å^2. The effective area density is

$$\rho h = \frac{M}{S} = 5.908 \times 10^{-4} \frac{\text{eV ps}^2}{\text{Å}^2},$$

(2)

where ρ and h are the effective bulk density and ring thickness.

2. ELASTIC RING MODEL

Before pressure $p(t)$ is applied, a perfectly circular ring performs small-amplitude free oscillations in its plane. These free vibrations will be represented as a sum of a few first harmonics. It is assumed that the pressure begins to act at the time of the greatest deviation for each harmonic. Then the initial conditions with respect to the deflection function $w(\theta,t)$, where θ is the central angle, are taken in the form

$$w(\theta,0) = \sum_{m=2} W_m^0 \cos(m\theta),$$
$$\dot{w}(\theta,0) = 0, \quad \sum_{m=2} W_m^0 = W_2^0 (m-1)^{-\alpha}, \quad \alpha \ge 0,$$

(3)

where m is the harmonic number, $W_2^{\,0}$ is the initial amplitude of the harmonic m=2. The overdot denotes the derivative with respect to time t. The uniform distribution of the amplitudes $W_m^{\,0}$ corresponds to α=0 and for α>0 the amplitude decreases with the harmonic number.

The linear equation of motion of the ring in its plane with respect to the deflection function $w(\theta,t)$ has the form [14]:

$$\frac{\partial^6 w}{\partial \theta^6} + 2\frac{\partial^4 w}{\partial \theta^4} + \frac{\partial^2 w}{\partial \theta^2} + 3\eta\left(\frac{\partial^4 w}{\partial \theta^4} + \frac{\partial^2 w}{\partial \theta^2}\right) + \frac{R^4}{\xi^2}\left(\frac{\partial^2 \dot{w}}{\partial \theta^2} - \dot{w}\right) = 0,$$

$$\eta = \frac{p}{p_2^*}, \quad p_2^* = \frac{3D}{R^3}, \quad \xi^2 = \frac{D}{\rho h}, \quad D = \frac{Eh^3}{12(1-\nu^2)}.$$

(4)

Here, D is the effective bending stiffness, E and ν are the effective modulus of elasticity and Poisson's ratio, respectively, p_2^* is the critical pressure at which the loss of stability of the circular shape of the ring with respect to the lowest harmonic m=2 occurs (it is indicated as p_1 above [10]). Since the width of the ring b enters the values of masses, stiffness and pressure, it is canceled in Eq. (4).

Eq. (4) does not take into account the influence of the surrounding gas environment, which is characterized by the parameter $\rho_f R\Delta/(\rho h)$, where ρ_f is the density of the surrounding medium, Δ is a complex function of the input quantities [14, 15]. The real and imaginary parts of Δ are responsible for the added mass of the medium and the radiation of energy from the tube. Except in special cases not covered here, Δ does not increase the value of this parameter. Therefore, the influence of the external environment on the motion

of the tube can be judged by the dimensionless parameter $\rho_f R\Delta/(\rho h)$. If its value is much less than one, then the influence of the environment is small. Taking into account the above value of ρh and the equality $2\pi R \approx aN$, this condition can be written as $\rho_f R \sim 10^{-6}$ kg/m^2 or $\rho_f N = 4 \times 10^4$ kg/m^3. For air at atmospheric pressure $\rho_f = 1.2$ kg/m^3, and this condition gives $R \sim 10^3$ nm or $N = 3 \times 10^4$. We will consider the dynamics of a ring formed from atoms of order 10 to 100. Therefore, we will not take into account the influence of the external environment. With a slow increase in pressure on the tube, the considered influence of the medium on the tube is absent.

3. MOLECULAR DYNAMICS MODEL

CNT under plane strain conditions can be simulated with the use of the chain model proposed in [35, 36] and adapted for simulation of CNTs in [37, 38].

The chain model considers one zigzag row of carbon atoms moving in the *xy*-plane as shown in Fig. 1(b). The atoms are numbered with the index $i=1,\ldots,N$; their positions are defined by the radius-vectors r_i. The Hamiltonian of the chain is

$$H = \frac{M}{2}\sum_{i=1}^{N}|\dot{r}_i|^2 + U_B + U_A,\qquad(5)$$

where the first term gives the kinetic energy of the chain and the terms U_B and U_A describe the potential energy of valence bonds and valence angles, respectively.

The energy of valence bonds is

$$U_B = \sum_{i=1}^{N}\frac{\psi}{2}(|r_{i+1} - r_i| - a)^2 ,\qquad(6)$$

where $\psi = 25.279$ eV/Å^2 is the valence bond stiffness.

The energy of valence angles is

$$U_A = \sum_{i=1}^{N}\tau[1 + \cos\theta_i],\qquad \cos\theta_i = \frac{(r_i - r_{i-1}, r_{i+1} - r_i)}{|r_i - r_{i-1}||r_{i+1} - r_i|},\qquad(7)$$

where $\tau = 0.00166$ eV is the valence angle stiffness.

External forces applied to each atom were added to the equations of motion following from the Hamiltonian Eq. (5) to simulate a uniform conservative external pressure $p(t)$.

The chain model was successfully used for simulation of carbon nanostructures, in particular, structure and thermomechanical properties of CNT bundles were analyzed in the works [37, 40-45], folded and scrolled packings of carbon nanoribbons in [46], crumpled graphene under compression in [47]. Chain model can also be applied to the analysis of other two-dimensional nanomaterials [48, 49].

For N carbon atoms of the CNT cross section numbered by the index i (see Fig. 1(b)) the radial displacements can be presented as the sum of $N/2+1$ Fourier harmonics

$$w_i = \frac{1}{N}f_0 + \frac{1}{N}f_{N/2}\cos(\pi i) + \frac{2}{N}\sum_{m=1}^{N/2-1}\left[f_m\cos\left(\frac{2\pi m i}{N}\right) + g_m\sin\left(\frac{2\pi m i}{N}\right)\right],\qquad(8)$$

where the coefficients of the expansion are calculated as follows

$$f_m = \sum_{i=0}^{N-1} w_i \cos\left(\frac{2\pi mi}{N}\right), \quad m = 0,...,N/2,$$

$$g_m = \sum_{i=0}^{N-1} w_i \sin\left(\frac{2\pi mi}{N}\right), \quad m = 1,...,N/2-1. \tag{9}$$

The following initial radial displacements are applied

$$w_i = \sum_{m=2}^{4} W_m^0 \cos\left(\frac{2\pi mi}{N}\right),$$

$$\dot{w}_i = 0. \tag{10}$$

It can be seen that initially only three first bending harmonics shown in Fig. 2 are excited (the harmonics $m=0$ and $m=1$ are tensile and translational, respectively). We take equal amplitudes for the three harmonics, $W_m^0 = 10^{-3}R$, $m=2,3,4$, which is an analog of Eq. (3) for $\alpha=0$.
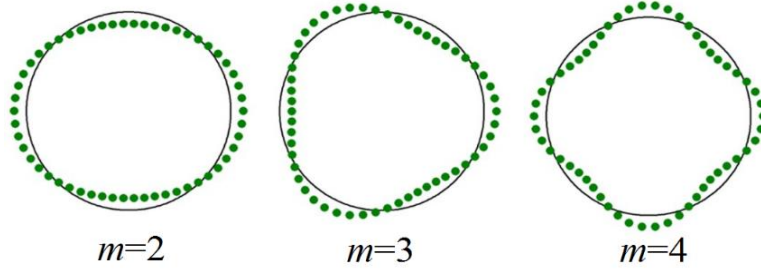
Fig. 2 The three first radial vibrational modes of the CNT cross section

Table 1 CNT radius R (in Å) and numerical values of ξ (in Å^2/ps) for various N and $m=2,3$ and 4.

N	R	ξ ($m=2$)	ξ ($m=3$)	ξ ($m=4$)
18	3.179	54.75	52.84	52.71
30	5.278	56.71	56.03	54.78
42	7.382	57.55	57.09	56.45
54	9.487	57.84	57.55	57.18
66	11.59	57.98	57.78	57.49
78	13.70	58.06	57.92	57.74
90	15.80	58.12	58.01	57.86
102	17.91	58.15	58.07	57.95
114	20.02	58.18	58.11	58.02
126	22.12	58.19	58.14	58.07
138	24.23	58.21	58.17	58.11
150	26.33	58.22	58.19	58.14

The amplitudes of $N/2+1$ Fourier harmonics are

$$
\begin{aligned}
W_0 &= |f_0|, \\
W_m &= \sqrt{f_m^2 + g_m^2}, \quad m = 1, ..., N/2 - 1,, \\
W_{N/2} &= |f_{N/2}|.
\end{aligned}
\tag{11}
$$

Numerical examples will be given for the CNT with the number of atoms N=200. For such a large value of N we take ξ=58.2 Å^2/ps, see Table 1. From Eq. (1) one finds the CNT radius $R = aN/(2\pi)$=35.08 Å and from Eqs. (2) and (4) D=2.001 eV.

The equations of motion of the atoms representing the CNT cross section are integrated numerically by the symplectic Stormer method of the sixth order of accuracy [39]. Time evolution of the Fourier harmonic amplitudes, $W_m(t)$, is analyzed.

4. NATURAL VIBRATION FREQUENCIES OF CNT

The theory of thin elastic shells gives the following expression for the natural circular frequencies of bending vibrations of a cylindrical shell [14]

$$
\Omega_m = \frac{m(m^2 - 1)\xi}{R^2 \sqrt{m^2 + 1}},
\tag{12}
$$

where $m \geq 2$ is the harmonic number and R is the shell radius.

The numerical values of the parameter ξ included in Eqs. (4) and (12) were determined in [40, 41] by comparing the frequencies Ω_m by Eq. (12) and by the chain model; they are given in Tab. 1. The analytical approximation $\xi(N,m)$ given in [41] gives a satisfactory result only for the mode m=2. Here, this approximation is somewhat improved and has the form

$$
\xi(N, m) = A - (sm - q)N^{-5/2},
\tag{13}
$$

where A=58.2 Å^2/ps, s=7.2×10^3 Å^2/ps, q=8.4×10^3 Å^2/ps. For N>150 and $m \leq 4$ the value ξ=58.2 Å^2/ps remains constant.

In Fig. 3, the dependencies $\xi(N,m)$ according to Eq. (13) are given for m=2,3 and 4 together with the numerical data (scattered) obtained with the help of the chain model. The value of ξ increases with an increase in the number of atoms N and decreases with an increase in the harmonic number m.

The ratio of the wavelength around the circumference of the ring $2\pi R/m \approx aN/m$ to the thickness h is $aN/(mh)$. Taking into account the value of a=1.102 Å and the value of h=3.3 Å, which is the interlayer distance in graphite, we obtain this ratio equal to $N/(3m)$. Equation of motion Eq. (4), based on the Kirchhoff hypotheses [14], is valid for $N/(3m)$>10. It was obtained without taking into account the inertia of rotation of the ring element and transverse shear, which affect the solution for $N/(3m)$<10. In this case, it is necessary to use the Timoshenko model, which takes these factors into account [50, 51].

On the other hand, at $N/(3m)$<10, there are less than 15 atoms per half-wavelength, and the inaccuracy of the equations of continuum mechanics becomes noticeable. Taking into account the inertia of rotation and transverse shear leads to a decrease in the natural

vibration frequencies in comparison with the result based on Kirchhoff hypotheses. This trend is seen in Fig. 3.
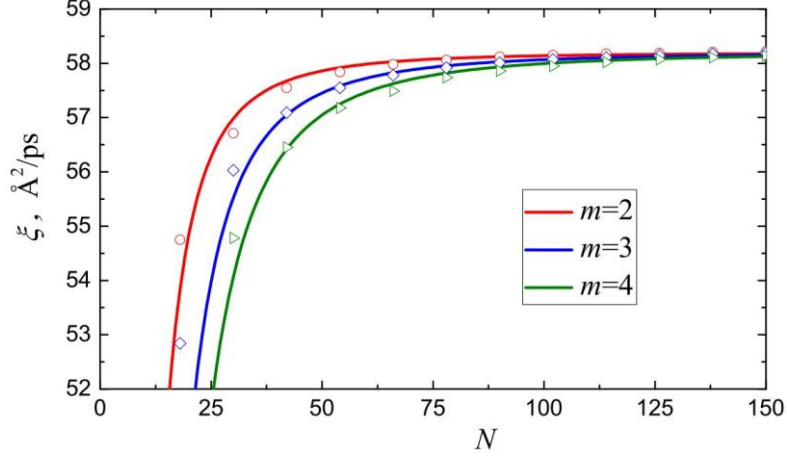
Fig. 3 Dependence of the parameter ξ entering Eq. (13) on the number of atoms N forming a single-layer ring and the harmonic number m of radial vibrations. The dots show the numerical values from [18].

5. LONG-TERM PRESSURE RESPONSE

At $t=0$ the external pressure $p=const$ is instantly applied to the CNT and acts for a long time. By a long duration of a pressure pulse of constant intensity, we mean a time interval $t<\tau$, an order of magnitude or more exceeding the oscillation period $2\pi/\omega_m$.

5.1 Analytical Treatment

Looking for a solution to equation Eq. (4) in the form

$$w = \sum_{m=2} W_m(t)\cos(m\theta),\qquad(14)$$

from Eq. (4) and Eq. (14) we obtain

$$\ddot{W}_m + \omega_m^2 W_m = 0,\qquad(15)$$

were

$$\omega_m^2 = \Omega_m^2\left(1 - \frac{3\eta}{m^2-1}\right),\qquad(16)$$

Here, Ω_m is the natural frequency of the m-th harmonic at zero pressure defined by Eq. (12), ω_m is the frequency under the action of excess pressure p.

The critical pressure value for the CNT with $N=200$, $R=35.08$ Å, and $D=2.001$ eV, with respect to the harmonic $m=2$, in accordance with Eq. (4), is

$$p_2^* = \frac{3D}{R^3} = 1.391 \times 10^{-4}\, \frac{eV}{\mathring{A}^3} = 22.28\, MPa\ . \tag{17}$$

From the condition $\omega_m = 0$ one finds from Eq. (16) the critical values of pressure for other harmonics,

$$p_m^* = p_m^* \frac{m^2 - 1}{3}\ , \tag{18}$$

and hence, for the considered CNT,

$$p_3^* = \frac{8}{3} p_2^* = 3.709 \times 10^{-4} = 59.41\, MPa \tag{19}$$

$$p_4^* = 5 p_2^* = 6.955 \times 10^{-4} = 111.4\, MPa \tag{20}$$

Next, we analyze the CNT dynamics after an instantaneously applied constant external pressure p. In the case of an abrupt increase in pressure at time $t=0$ from 0 up to a constant value p, the solution to Eq. (15) has the form

$$W_m(t) = A_m e^{\omega_m t} + B_m e^{-\omega_m t}\ . \tag{21}$$

Satisfying the initial conditions Eq. (3), we obtain for the m-th harmonic

$$\frac{W_m(t)}{W_m^0} = \begin{cases} \cos(\omega_m t), & 3\eta < m^2 - 1, \\ \cosh(\omega_m t), & 3\eta > m^2 - 1. \end{cases} \tag{22}$$

Thus, depending on the ratio of the effective pressure to the critical pressure η and the number of the harmonic m, oscillations or/and an exponential growth of the initial deflections can be excited after the load is applied. For a relatively small value of $p < p_m^* = p_2^*(m^2-1)/3$, the first, time periodic solution in Eq. (22) is realized for the harmonic m. For example, for harmonic $m=3$ this condition is $p < (8/3)p_2^*$ and for $m=4$ this condition is $p < 5p_2^*$. In the case of a large value of the effective pressure, for one or several lowest harmonics the second solution in Eq. (22) takes place. The harmonic number m_R separating these lowest modes of motion is determined from the condition $\omega_m = 0$ and is equal to

$$m_R = \left\lfloor \sqrt{1 + 3\eta} \right\rfloor, \tag{23}$$

where $\lfloor \cdot \rfloor$ denotes the round down operation.

Solution Eqs. (14) and (22), can be written as

$$\frac{w}{W^0} = \left[\sum_{m=2}^{m_R} (m-1)^{-\alpha} \cosh(\omega_m t) + \sum_{m=m_R+1}^{\infty} (m-1)^{-\alpha} \cos(\omega_m t) \right] \cos(m\theta)\ . \tag{24}$$

It can be seen from Eq. (24) that the first harmonics from the 2nd to m_R show an exponential increase in amplitude with time, and the larger ω_m, the faster the growth. Harmonics above m_R oscillate with frequency ω_m.

The fastest growth of the amplitude occurs for the harmonic with the number $m=m_L$, determined from the condition $d\omega_m /dm=0$. In the simplest case of the independence of the parameter ξ from n ($N>78$) and the same initial deviation amplitudes ($\alpha=0$) this condition gives

$$m_L \approx \left\lceil \frac{1}{2}\sqrt{m_R^2 - 2 + m_R\sqrt{m_R^2 + 12}} \right\rceil, \qquad (25)$$

where $\lceil \cdot \rceil$ denotes the round up operation. The m_L value is somewhat less than the m_R value. Therefore, the fastest increase in the amplitude is observed for the harmonic at the border of exponential growth and oscillatory motion. What has been said applies to the case of a uniform distribution of the initial deviation over harmonics ($\alpha=0$). At $\alpha>0$, the picture changes. At the beginning of the process, the harmonic with number $m=2$ prevails due to the nature of the initial conditions Eq. (3) and the presence of the factor $(m-1)^{-\alpha}$ in solution Eq. (24). With increasing time, the second term in Eq. (24), $2^{-\alpha}\cosh(\omega_3 t)$ becomes larger than the first, $\cosh(\omega_2 t)$, and so on.

Thus, during dynamic deformation of a CNT with a decreasing distribution of small initial deflection over harmonics, a rearrangement in m occurs over time. At large time, the harmonic m_L, which is determined approximately by Eq. (25), becomes dominant. In the presence of limiters of movement along the radius, for example, contacting media, the harmonic m_L may not become dominant. Nonlinearities can also lead to this limitation.

5.2 Chain Model Results

Let us first check the accuracy of Eq. (16) in predicting the main frequency of CNT vibrations at an external pressure $p<p_2^*$, i.e. for $\eta<1$.

Molecular dynamics modeling is carried out as follows. The initial condition Eq. (10) is applied to the CNT at pressure p, and the time evolution of the harmonic amplitudes $m=2,3$ and 4 is calculated from Eq. (11).

In Fig. 4(a) time evolution of the harmonic amplitudes W_2, W_3 and W_4 is presented for CNT with $N=200$ at pressure $p=1.14\times10^{-4}$ eV/Å^3 $= 18.2$ MPa. In view of Eq. (17), one finds the analytical value of $\eta=p/p_2^*=0.816$. From the numerically obtained function $W_2(t)$ one finds the oscillation frequency of the second harmonic as $\omega_2=54.6$ GHz. From Eq. (12) it follows that the natural vibration frequency of the second harmonic is $\Omega_2=126.9$ GHz. From Eq. (16), for $m=2$ one has $\eta=1 - (\omega_2/\Omega_2)^2=0.815$, which is in a very good agreement with the analytical estimation.

Similar numerical results were obtained for different pressure values, they are presented in Fig. 4(b) by black squares. The red line shows the analytical dependence $\omega_2/\Omega_2=(1-\eta)^{1/2}$, which follows from Eq. (16) for $m=2$. It can be seen that the theory predicts very well the dependence of the fundamental oscillation frequency on the applied external pressure in the studied case of $\eta<1$ amplitudes of all harmonics are periodic functions of time.

Next, we analyze the case $\eta>1$, in particular, consider $\eta=2,3$ and 7.

For $\eta=2$, $p>p_2^*$ and $p<p_m^*$ for $m>2$. From Eqs. (23) and (25) for $\eta=2$ we find $m_R=\lceil 2.6 \rfloor$ and $m_L=\lceil 2.0 \rceil$. Rounded values are $m_R=3$ and $m_L=2$. According to the above theory, in Eq. (24) the first sum is taken from 2 to 3, and the second - from 4. The harmonic $m=2$ grows exponentially with time and is the fastest growing harmonic. The remaining harmonics are periodic in time. In Fig. 5(a), the time dependence of the harmonic amplitudes is presented.

In line with the theoretical prediction, W_2 grows exponentially, while W_3 and W_4 fluctuate over time.
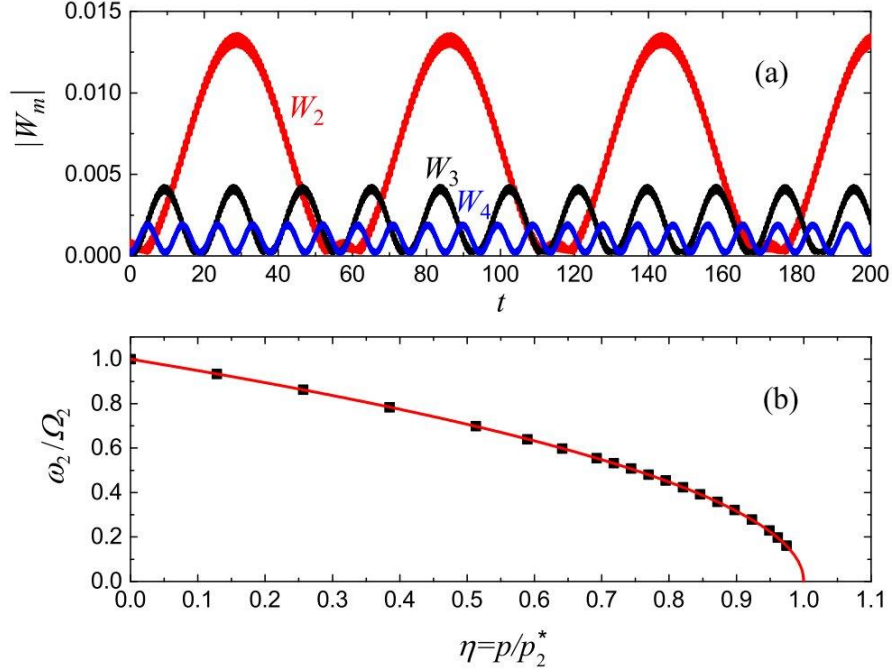
Fig. 4 (a) Amplitudes of Fourier harmonics as the functions of time found for CNT with $N=200$ under external pressure $p=18.2$ MPa ($\eta=p/p_2^*=0.816$). (b) Frequency of the harmonic $m=2$ normalized to the natural vibration frequency at $p=0$ as the function of the applied pressure normalized to the critical value p_2^*. Red line shows the analytical solution Eq. (16) for the elastic ring and black squares the numerical results for the CNT.

For $\eta=3$, $p>p_3^*$ and $p<p_m^*$ for $m>3$. From Eqs. (23) and (25) for $\eta=3$ we find $m_R=\lfloor 3.4 \rfloor$ and $m_L=\lceil 2.4 \rceil$. Rounded values are $m_R=3$ and $m_L=3$. As can be seen from Fig. 5(b), W_2 and W_3 grow exponentially, while W_4 performs oscillations. As predicted by the theory, the fastest growth is demonstrated by W_3.

For $\eta=7$, $p>p_4^*$ and $p<p_m^*$ for $m>4$. From Eqs. (23) and (25) for $\eta=7$ we find $m_R=\lfloor 4.7 \rfloor$ and $m_L=\lceil 3.4 \rceil$. Rounded values are $m_R=4$ and $m_L=4$. In Eq. (24), the first sum is taken from 2 to 4, and the second from 5. The harmonics $m=2,3$ and 4 grow exponentially, with the fastest growing harmonic $m=4$. The numerical results are presented in Fig. 5 (c) to confirm the theoretical predictions. Starting from $m=5$, oscillations occur with increasing frequency and decreasing amplitude around the motion determined by the harmonics $m=2,3$ and 4.
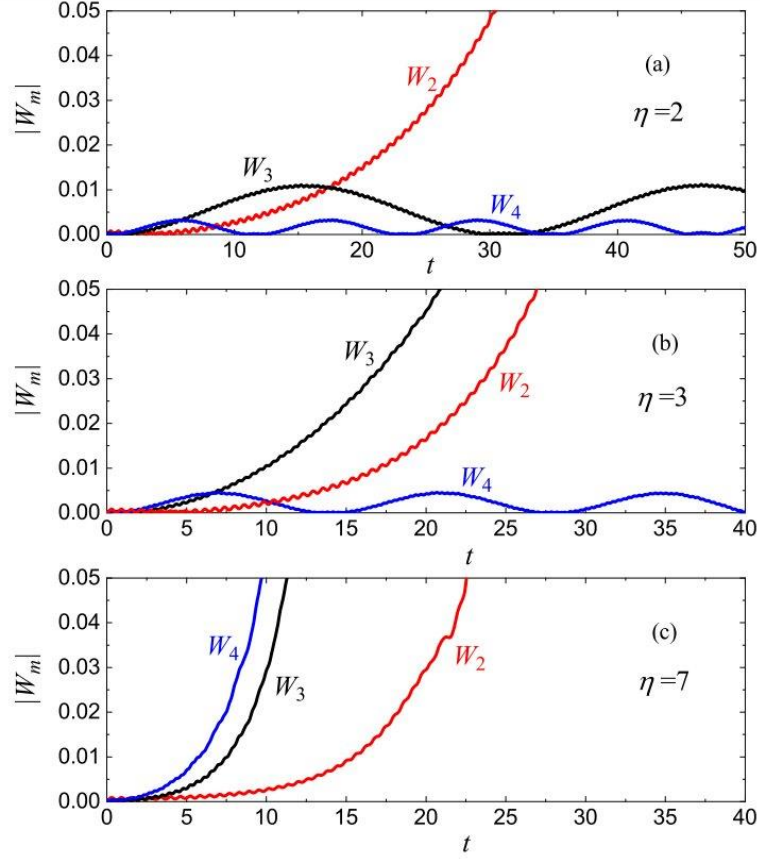
Fig. 5 (a) Amplitudes of Fourier harmonics as the functions of time found for CNT with
N=200 under external pressure p corresponding to (a) η=2, (b) η=3, and (c) η=7.

6. REACTION TO A PRESSURE PULSE

Below we analyze the dynamics of CNTs due to a relatively short rectangular pressure pulse.

6.1 Analytical Treatment

In the case of the pressure pulse shown in Fig. 6, one can use solution Eq. (24) within $0 \leq t \leq \tau$, where τ is the pulse duration. For $t > \tau$, when p=0, η=0, $\omega_n = \Omega_n$, the solution to Eq. (15) has the form

$$W_m(t) = A_m \cos(\Omega_m t) + B_m \sin(\Omega_m t) . \qquad (26)$$

The integration constants are determined from the conditions

$$\frac{W_m(t)}{W_m^0} = \begin{cases} \cos(\omega_m\tau), & 3\eta < m^2 - 1, \\ \cosh(\omega_m\tau), & 3\eta > m^2 - 1, \end{cases}$$

$$\frac{\dot{W}_m(t)}{W_m^0} = \begin{cases} -\omega_m \sin(\omega_m\tau), & 3\eta < m^2 - 1, \\ \omega_m \sinh(\omega_m\tau), & 3\eta > m^2 - 1. \end{cases} \tag{27}$$

The first line in $W_m(t)$ and $\dot{W}_m(t)$ corresponds to the case when the effective pressure $p < p_2^*(m^2-1)/3$, see Fig. 6(a), and the second line is valid in the opposite case, see Fig. 6(b).
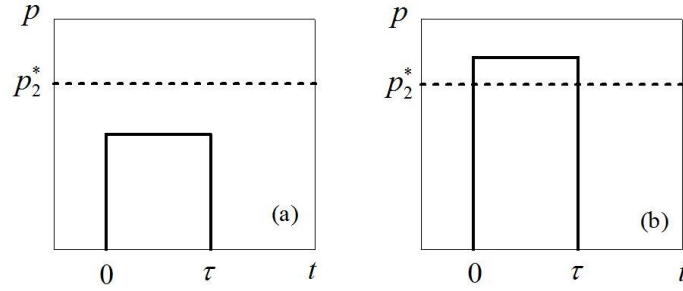
Fig. 6 A rectangular pressure pulse with a height (a) less than the critical pressure p_2^*, (b) greater than the critical pressure. The pulse duration is τ.

The dynamics of the ring after the termination of the action of the pressure pulse ($t > \tau$) is determined by the expressions

$$\frac{W_m(t)}{W_m^0} = \begin{cases} \cos(\omega_m\tau)\cos[\Omega_m(t-\tau)] - \beta_m \sin(\omega_m\tau)\sin[\Omega_m(t-\tau)], & \beta_m^2 > 0, \\ \cosh(\omega_m\tau)\cos[\Omega_m(t-\tau)] + i\beta_m \sinh(\omega_m\tau)\sin[\Omega_m(t-\tau)], & \beta_m^2 < 0, \end{cases} \tag{28}$$

where i is the imaginary unit and we have introduced the notation

$$\beta_m^2 = 1 - \frac{3\eta}{m^2 - 1} \tag{29}$$

in accordance with Eq. (16), so that $\omega_m^2 = \beta_m^2 \Omega_m^2$. For $\tau=0$ in both solutions of Eq. (28), the motion is a continuation of the initial motion defined by Eq. (3), $w = \Sigma W_{0m}\cos(\Omega_m t)\cos(m\theta)$, since there is no pressure drop yet. In the case $p=0$ ($\eta=0$, $\beta_m=\pm 1$) from the first solution we obtain the same function, and the second solution Eq. (15) has no meaning. In the general case, the motion in the interval $0 < t < \tau$ is determined by Eq. (24), and for $t > \tau$ by Eq. (28).

Thus, during the pressure action ($0 < t < \tau$), when $3p < p_2^*(m^2-1)$, oscillations occur with frequencies ω_m and amplitudes W_m^0. After the cessation of the pressure ($t > \tau$), oscillations for each harmonic occur with a higher frequency Ω_m than ω_m.

In the case $3p > p_2^*(m^2-1)$, within the pressure pulse ($0 < t < \tau$), an exponential growth of the harmonic amplitudes occurs. At $t > \tau$, oscillations occur with the same frequencies Ω_m, but with increased amplitudes. This solution is valid within the formulation of the problem in the linear approximation.

Example. Let us consider in more detail the dynamics of the harmonic $m=2$ in the CNT with the number of atoms $N=200$. According to Eq. (12), $\Omega_2=0.127$ rad/ps. For $p=18.2$ MPa ($\eta=p/p_2^*=0.816$, $\beta_2=0.429$) one has from Eq. (16) $\omega_2=0.054$ rad/ps. Since $p<p_2^*$, the first line of Eq. (28) applies,

$$\frac{W_2}{W_2^0} = \begin{cases} \cos(0.054t), & 0 \le t < \tau, \\ \cos(0.054\tau)\cos[0.127(t-\tau)]+0.429\sin(0.054\tau)\sin[0.127(t-\tau)], & (t > \tau). \end{cases} \tag{30}$$

In this case, the oscillation amplitude after the termination of the pressure does not depend on its duration τ.

Now we consider the case of $\eta>1$. Let us take $\eta=1.1$, then $\beta_2=(p/p_2^*-1)^{1/2}=0.316$, $\omega_2=\Omega_2\beta_2=0.040$ rad/ps. For $t<\tau$ the solution is given by Eq. (24) and for $t>\tau$ the solution is given by the second line of Eq. (28):

$$\frac{W_2}{W_2^0} = \begin{cases} \cosh(0.040t), & 0 \le t < \tau, \\ \cosh(0.040\tau)\cos[0.127(t-\tau)]-0.316\sinh(0.040\tau)\sin[0.127(t-\tau)], & (t > \tau). \end{cases}$$
$$\tag{31}$$

It is clear that for $p>p_2^*$ there is a strong dependence of the amplitude of oscillations after the termination of pressure pulse on its duration τ.

6.2 Chain Model Results

The time dependence of the harmonic amplitudes W_2, W_3 and W_4, are shown for the CNT with $N=200$ for the pulsed pressure in Fig. 7.

In Fig. 7(a) $p=18.2$ MPa ($\eta=0.816$) and pulse duration is equal to $\tau=100$ ps. This result should be compared with the one shown in Fig. 4(a), where the same pressure is constantly applied. Under the action of a pressure pulse, the CNT wall performs periodic oscillations, and the fundamental bending harmonic $m=2$ has a frequency $\omega_2=0.054$ rad/ps. After the external pressure is removed, the amplitude of oscillations of the $m=2$ harmonic decreases somewhat, and the frequency increases in accordance with the theoretical prediction, see the first line of Eq. (28). Removing the pressure has little effect on the dynamics of higher harmonics $m=3$ and 4.

In panels (b) and (c) of Fig. 7, the external pressure is greater than p_2^*, namely, it corresponds to $\eta=2$ and 3, respectively. The duration of the pressure pulse is $\tau=25$ and 20 ps, respectively. These graphs should be compared with Fig. 5(a) and (b) respectively, where the same pressure is constantly applied. It can be seen from Fig. 7 that after the removal of external pressure, the exponential growth of W_2 in (b) and W_2 and W_3 in (c) turns into a periodic motion with an amplitude reached by the time τ. This means that the oscillation amplitude of these harmonics strongly depends on τ, as it was shown theoretically, see the second line of Eq. (28).

It can be concluded that the theory of thin shells describes very well the dynamics of CNTs under pulsed pressure. This conclusion is supported by comparison of the critical pressure values calculated using molecular dynamics and the shell theory, see Fig. 4(b), and also by the dynamics of various harmonics under constant and pulsed pressure, see Fig. 5 and Fig. 7.
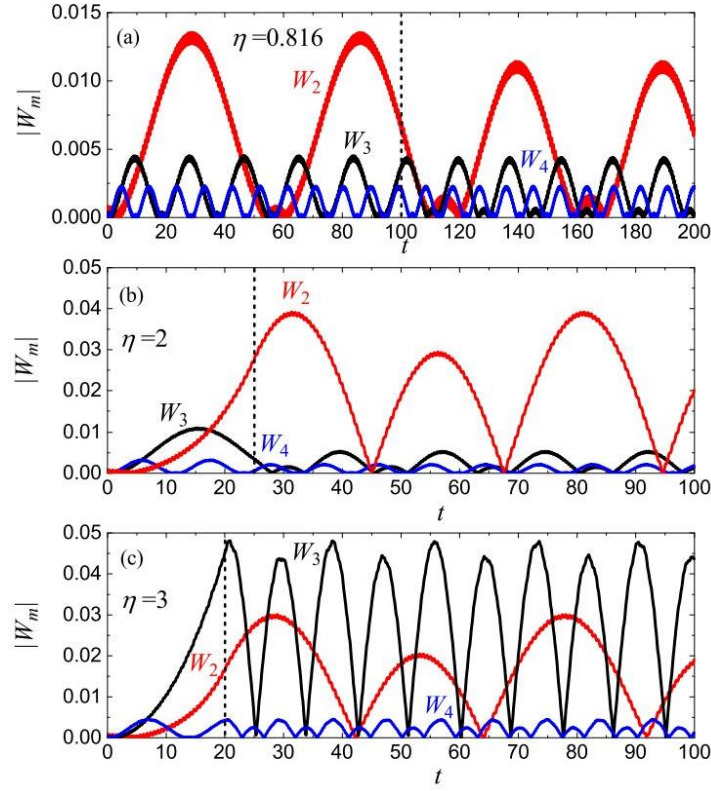
Fig. 7 (a) Amplitudes of Fourier harmonics as the functions of time found for CNT with N=200 under external pulsed pressure (a) p=18.2 MPa (η=0.816), (b) p=36.4 MPa (η=2.0), and (c) p=54.6 MPa (η=3.0). Pressure drops to zero at time τ shown by the vertical dashed line: in (a) τ=100 ps, (b) τ=25 ps, and (c) τ=20 ps.

5. Conclusions

At present, the static deformation of the CNT cross section under the action of external pressure has been studied and a strong dependence on the CNT diameter has been shown. The spectral properties of the nanotubes were also analyzed depending on the external pressure. To the best of our knowledge, the dynamic behavior of CNTs under the action of a pressure pulse of various durations and intensities has been less studied. In this work, to analyze the dynamics of CNTs under plane strain conditions, we applied a continuum approach based on the theory of thin cylindrical shells based on the Kirchhoff hypotheses. In addition, we used the molecular dynamics method based on the chain model, which describes the deformation of the CNT cross section under a uniform external pressure. By comparing the eigenfrequencies of radial vibrations of a circular ring and CNT wall consisting of a different number of atoms N, the parameter ξ is determined, which contains the bending stiffness and density of the ring, see Table 1.

The introduction of the parameter ξ into the analysis opens up the possibility of a wide application of the models and relations of the well-developed theory of elastic thin shells. In this case, it is not necessary to involve such parameters as effective density, elastic modulus, Poisson's ratio, wall thickness, the determination of which is a difficult task. Determining the parameter ξ from such an integral characteristic as natural frequencies of CNT vibrations seems to be more justified than from the effective parameters, which are given in the literature with a wide spread. For example, the effective thickness of the CNT wall is given in the literature in the range 0.7-3.4 Å.

From the analysis of the values of the parameter ξ for CNTs of different diameters, determined by the chirality index n (or number of carbon atoms in a CNT cross section $N=2n$) given in Table. 1, one can conclude that for the zigzag CNTs $(n,0)$ with $n>15$, in the regime of small amplitude vibrations, the discrepancy between the continuum model and molecular dynamics calculations does not exceed 5% and decreases with increasing n.

As a result of the theoretical analysis carried out within the framework of the linear theory of thin shells, the dynamics of the deflection function of the CNT wall is described under the instantaneous application of a time constant or pulsed external pressure. Theoretical results are compared with molecular dynamics calculations, where the expansion of the deflection function in a Fourier series was analyzed.

In particular, it is shown that the dynamics of bending harmonics with numbers $m\geq2$ changes qualitatively when the external pressure exceeds the critical values p_m^* determined from Eq. (18). At pressure in the range $p_m^* < p < p_{m+1}^*$, the amplitude of harmonics with numbers less than $m+1$ grows exponentially, while harmonics with higher numbers exhibit oscillatory motion. Interestingly, the fastest increase in the amplitude is observed for the harmonic at the border of exponential growth and oscillatory motion.

Under the action of a rectangular pressure pulse of short duration (compared to the oscillation period of the fundamental bending harmonic), the dynamics of different modes depends both on the value of the applied pressure p and on the pulse duration τ. For oscillating harmonics, the amplitude of oscillations after the termination of the pressure pulse weakly depends on τ, and for harmonics whose amplitude grows exponentially with time, the amplitude of oscillations at $t > \tau$ increases rapidly with increasing τ.

The results presented in our work deepen our understanding of the dynamics of CNTs under the action of pulsed pressure. In the future, similar studies will be performed for spherical particles (fullerenes) [52-54].

REFERENCES

1. Harik, V.M., 2001, *Ranges of applicability for the continuum beam model in the mechanics of carbon nanotubes and nanorods*, Solid State Communications, 120(7-8), pp. 331-335.
2. Qian, D., Wagner, G.J., Liu, W.K., Yu, M.-F., Ruoff, R.S., 2002, *Mechanics of carbon nanotubes,* Applied Mechanics Reviews, 55(6), pp. 495-532.
3. Yu, M.-F., 2004, *Fundamental mechanical properties of carbon nanotubes: Current understanding and the related experimental studies*, Journal of Applied Mechanics and Technical Physics, 126(3), pp. 271-278.

4. Annin, B.D., Baimova, Y.A., Mulyukov, R.R., 2020, *Mechanical properties, stability, and buckling of graphene sheets and carbon nanotubes (review)*, Journal of Applied Mechanics and Technical Physics, 61(5), pp. 834-846.

5. Khadimallah, M.A., Hussain, M., Taj, M., Ayed, H., Tounsi, A., 2021, *Parametric vibration analysis of single-walled carbon nanotubes based on Sanders shell theory*, Advances in Nano Research, 10(2), pp. 165-174.

6. Zhao, Z.S., Zhou, X.-F., Hu, M., Yu, D.L., He, J.L., Wang, H.-T., Tian, Y.J., Xu, B. J., 2012, *High-pressure behaviors of carbon nanotubes Superhard*, Journal of Superhard Materials, 34(6), pp. 371-385.

7. Khaniki, H.B., Ghayesh, M.H., Amabili, M., 2021, *A review on the statics and dynamics of electrically actuated nano and micro structures*, International Journal of Non-Linear Mechanics, 129, 103658.

8. Peters, M., McNeil, L., Lu, J.P., Kahn D., 2000, *Structural phase transition in carbon nanotube bundles under pressure*, Physical Review B, 61, pp. 5939-5944.

9. Teredesai, P.V., Sood, A.K., Muthu, D.V.S., Sen, R., Govindaraj, A., Rao, C.N.R., 2000, *Pressure-induced reversible transformation in single-wall carbon nanotube bundles studied by Raman spectroscopy*, Chemical Physics, 319 (3-4), pp. 296-302.

10. Wu, J., Zang, J., Larade, B., Guo, H., Gong, X.G., Liu, F., 2004, *Computational design of carbon nanotube electromechanical pressure sensors*, Physical Review B, 69, 153406.

11. Sun, D.Y., Shu, D.J., Ji, M., Liu, F., Wang, M., Gong, X.G., 2004, *Pressure-induced hard-to-soft transition of a single carbon nanotube*, Physical Review B, 70, 165417.

12. Merlen, A., Bendiab, N., Toulemonde, P., Aouizerat, A., San Miguel, A., Sauvajol, J.L., Montagnac, G., Cardon, H., Petit P., 2005, *Resonant Raman spectroscopy of single-wall carbon nanotubes under pressure*, Physical Review B, 72, 035409.

13. Molodets, A., Golyshev, A., Zhukov, A., Muradyan, V., Pisarev, S., Shulga, Y., Fortov, V., 2008, *Structural and morphological changes induced shock waves in carbon nanotubes*, Nanotechnologies in Russia, 3(11-12), pp. 697-703.

14. Seide, P., Jamjoom, T.M.M., 1974, *Large deformations of circular rings under nonuniform normal pressure*, Journal of Applied Mechanics, 41(1), pp. 192-196.

15. Bleich, H.H., Baron, M.L., 1954, *Free and forced vibrations of an infinitely long cylindrical shell in an infinite acoustic medium*, Journal of Applied Mechanics, 21(2), pp. 167-177.

16. Sirenko, Y.M., Stroscio, M.A., Kim, K.W., 1996, *Elastic vibrations of microtubules in a fluid*, Physical Review E, 53, pp. 1003-1010.

17. Kahn, D., Lu, J.P., 1999, *Vibrational modes of carbon nanotubes and nanoropes*, Physical Review B, 60, pp. 6535-6540.

18. Kitt, A.L., Qi, Z., Remi, S., Park, H.S., Swan, A.K., Goldberg, B.B., 2013, *How graphene slides: Measurement and theory of strain-dependent frictional forces between graphene and SiO$_2$*, Nano Letters, 13, pp. 2605-2610.

19. Kurti, J., Kresse, G., 1998, *First-principles calculations of the radial breathing mode of single-wall carbon nanotubes*, Physical Review B, 58, pp. R8869- R8872.

20. Goupalov, S.V., 2005, *Continuum model for long-wavelength phonons in two-dimensional graphite and carbon nanotubes*, Physical Review B, 71, 085420.

21. Shi, J.-X., Lei, X.-W., Natsuki T., 2021, *Review on carbon nanomaterials-based nano-mass and nano-force sensors by theoretical analysis of vibration behaviour*, Sensors, 21(5), pp. 1-22.

22. Li, C.-Y., Chou, T.-W., 2004, *Strain and pressure sensing using single-walled carbon nanotubes*, Nanotechnology, 15, 1493.

23. Ghaffari, S.S., Ceballes, S., Abdelkefi, A., Nonlinear Dynamics, 2020, *Nonlinear dynamical responses of forced carbon nanotube-based mass sensors under the influence of thermal loadings*, Nonlinear Dynamics, 100, pp. 1013-1035.

24. Natsuki, T., Urakami, K., 2019, *Analysis of vibration frequency of carbon nanotubes used as nano-force sensors considering clamped boundary condition*, Electronics, 8(10), 1082.

25. Menacer, F., Kadr, A., Dibi, Z., 2018, *Modeling of a smart nano force sensor using finite elements and neural networks*, International Journal of Automation and Computing, 17, pp. 279-291.

26. Schroeder, V., Savagatrup, S., He, M., Lin, S., Swager, T.M., 2019, Carbon nanotube chemical sensors, Chemical Reviews, 119 (1), pp. 599-663.

27. Sanaeepour, M., Abedi, A., Sharifi, M.J., 2017, *Performance analysis of nanoscale single layer graphene pressure sensors*, IEEE Transactions on Electron Devices, 64 (3), pp. 1300-1304.

28. Ahn, S.I., Jung, J.R., Choi, S.Y., Son, M.H., Hong, Y.J., Park, J.-C., 2017, *Ultra-sensitive graphene sensor for measuring high vacuum pressure*, Scientific Reports, 7, 12604.

29. Sorkin, V., Zhang, Y.W., 2011, *Graphene-based pressure nano-sensors*, Journal of Molecular Modeling volume, 17, pp. 2825-2830.

30. Cao, G., 2014, *Atomistic Studies of Mechanical Properties of Graphene*, Polymers, 6(9), pp. 2404-2432.

31. Wang, S., Gao, E., Xu, Z., 2019, *Interfacial failure boosts mechanical energy dissipation in carbon nanotube films under ballistic impact*, Carbon, 146, pp. 139-146.
32. Xiao, K., Lei, X., Chen, Y., An, Q., Hu, D., Wang, C., Wu, X., Huang, C., 2021, *Extraordinary impact resistance of carbon nanotube film with crosslinks under micro-ballistic impact*, Carbon, 175, pp. 478-489.
33. Zhao, Y., Miao, L., Hao, W., Zhao, G., Li, J., Jiaxuan, L., Liu, Z., Sui, C., He, X., Wang, C., 2021, *Two-dimensional carbon nanotube woven highly-stretchable film with strain-induced tunable impacting performance*, Carbon, 189, pp. 539-547.
34. Galiakhmetova, L.K., Bachurin, D.V., Korznikova, E.A., Bayazitov, A.M., Kudreyko, A.A., Dmitriev, S.V., 2022, *Shock loading of carbon nanotube bundle*, Mechanics of Materials, 174, 104460.
35. Savin, A.V., Korznikova, E.A., Dmitriev, S.V., 2020, *Twistons in graphene nanoribbons on a substrate*, Physical Review B, 102, 245432.
36. Savin, A.V., Korznikova, E.A., Krivtsov, A.M., Dmitriev, S.V., 2020, *Longitudinal stiffness and thermal conductivity of twisted carbon nanoribbons*, European Journal of Mechanics - A/Solids, 80, 103920.
37. Abdullina, D.U., Korznikova, E.A., Dubinko, V.I., Laptev, D.V., Kudreyko, A.A., Soboleva, E.G., Dmitriev, S.V., Zhou K., 2020, *Mechanical response of carbon nanotube bundle to lateral compression*, Computation, 8(2), 27.
38. Dmitriev, S. V., Ilgamov, M. A., 2021, *The radial response of a carbon nanotube to dynamic pressure*, Doklady Physics, 66, pp. 336-340.
39. Bakhvalov, N. S., 1977, *Numerical methods: analysis, algebra, ordinary differential equations*, MIR Publishers, Moscow, 663 p.
40. Dmitriev, S.V., Semenov, A.S., Savin, A.V., Ilgamov, M.A., Bachurin D.V., 2021, *Rotobreather in a carbon nanotube bundle*, Journal of Micromechanics and Molecular Physics, 5, 2050010.
41. Dmitriev, S.V., Sunagatova, I.R., Ilgamov, M.A., Pavlov, I.S., 2021, *Natural frequencies of bending vibrations of carbon nanotubes*, Technical Physics, 91(11), pp. 1732-1737.
42. Savin, A.V., Kivshar Yu.S., 2022, *Modeling of second sound in carbon nanostructures*, Physical Review B, 105(20), 205414.
43. Rysaeva, L.K., Bachurin, D.V., Murzaev, R.T., Abdullina, D.U., Korznikova, E.A., Mulyukov, R.R., Dmitriev, S.V., 2020, *Evolution of the carbon nanotube bundle structure under biaxial and shear strains*, Facta Universitatis-Series Mechanical Engineering, 18(4), pp. 525-536.
44. Savin, A.V., Korznikova, E.A., Dmitriev, S.V., 2022, *Plane vibrational modes and localized nonlinear excitations in carbon nanotube bundle*, Journal of Sound and Vibration, 520, 116627.
45. Savin, A.V., Korznikova, E.A., Dmitriev S.V., 2019, *Dynamics of surface graphene ripplocations on a flat graphite substrate*, Physical Review B, 99, 235411.
46. Savin, A.V., Korznikova, E.A., Dmitriev, S.V., 2015, *Simulation of folded and scrolled packings of carbon nanoribbons*, Physics of the Solid State, 57, pp. 2348-2355.
47. Baimova, J. A., Liu, B., Dmitriev, S. V., Zhou, K., 2015, *Mechanical properties of crumpled graphene under hydrostatic and uniaxial compression*, Journal of Physics D Applied Physics, 48(9), 095302.
48. Kosarev, I.V., Dmitriev, S.V., Semenov, A.S., Korznikova, E.A., 2022, *Stability of strained stanene compared to that of graphene,* Materials, 15(17), 5900.
49. Kosarev, I.V., Kistanov, A.A., Babicheva, R.I., Korznikova, E.A., Baimova, J.A., Dmitriev S.V., 2023, *Topological defects in silicene*, Europhysics Letters, 141(6), 66001.
50. Boumia L., Zidour M., Benzair A., Tounsi A., 2014, *A Timoshenko beam model for vibration analysis of chiral single-walled carbon nanotubes*, Physica E, 59, pp. 186-191.
51. Hsu, J.-C., Chang, R.-P., Chang, W.-J., 2008, *Resonance frequency of chiral single-walled carbon nanotubes using Timoshenko beam theory*, Physics Letters A, 372(16), pp. 2757-2759.
52. Erofeev, V.I., Pavlov, I.S., Porubov, A.V., Vasiliev, A.A., 2018, *Dispersion properties of a closed-packed lattice consisting of round particles*, Advanced Structured Materials, 90, pp. 101–117.
53. Erofeev, V.I., Pavlov, I.S., Leontiev, N.V., 2013, *A mathematical model for investigation of nonlinear wave processes in a 2D granular medium consisting of spherical particles*, Composites: Mechanics, Computations, Applications, 4(3), pp. 239–255.
54. Pavlov, I.S., Dmitriev, S.V., Vasiliev, A.A., Muravieva, A.V., 2022, *Models and auxetic characteristics of a simple cubic lattice of spherical particles*, Continuum Mechanics and Thermodynamics, 34(6), pp. 1669–1685.